Engineering 6 (2020) 1432–1442

Contents lists available at ScienceDirect

Engineering

journal homepage: www.elsevier.com/locate/eng

Research
Green Chemical Engineering—Perspective

Solvent-Less Vapor-Phase Fabrication of Membranes for Sustainable Separation Processes

Junjie Zhao [a,b], Karen K. Gleason [c,*]

[a] State Key Laboratory of Chemical Engineering, College of Chemical and Biological Engineering, Zhejiang University, Hangzhou 310027, China
[b] Institute of Zhejiang University–Quzhou, Quzhou 324000, China
[c] Department of Chemical Engineering, Massachusetts Institute of Technology, Cambridge, MA 02139, USA

ARTICLE INFO

Article history:
Received 3 May 2019
Revised 25 September 2019
Accepted 7 May 2020
Available online 13 May 2020

Keywords:
Membrane separation
Chemical vapor deposition
Atomic layer deposition
Molecular layer deposition
Thin films
Metal–organic frameworks
Polymers
Advanced manufacturing

ABSTRACT

Sustainable processes for purifying water, capturing carbon, producing biofuels, operating fuel cells, and performing energy-efficient industrial separations will require next-generation membranes. Solvent-less fabrication for membranes not only eliminates potential environmental issues with organic solvents, but also solves the swelling problems that occur with delicate polymer substrates. Furthermore, the activation procedures often required for synthesizing microporous materials such as metal–organic frameworks (MOFs) can be reduced when solvent-less vapor-phase approaches are employed. This perspective covers several vacuum deposition processes, including initiated chemical vapor deposition (iCVD), initiated plasma-enhanced chemical vapor deposition (iPECVD), solvent-less vapor deposition followed by *in situ* polymerization (SLIP), atomic layer deposition (ALD), and molecular layer deposition (MLD). These solvent-less vapor-phase methods are powerful in creating ultrathin selective layers for thin-film composite membranes and advantageous in conformally coating nanoscale pores for the precise modification of pore size and internal functionalities. The resulting membranes have shown promising performance for gas separation, nanofiltration, desalination, and water/oil separation. Further development of novel membrane materials and the scaling up of high-throughput reactors for solvent-less vapor-phase processes are necessary in order to make a real impact on the chemical industry in the future.

1. Introduction

The energy cost of separation processes in industry occupies 10%–15% of total energy consumption [1]. Membrane separation requires significantly less energy than the adsorption process and cryogenic distillations, and thus is a key component of sustainable processing and manufacturing. Moreover, unlike extraction and crystallization processes involving solvents, membrane processes eliminate the possibility of generating secondary contamination during the recycling and reprocessing of organic solvents. Therefore, membrane separations are ideal processes for green chemical engineering.

The working principle of membrane separation is based on the selective transport of different species through the membrane under a driving force. The selective sorption of one particular molecule over another and the different diffusion rates through the pores can both contribute to the selectivity of membrane separation [2]. Accordingly, precise functionalization within the membrane pores and fine-tuning of pore dimensions are desirable in order to achieve high selectivity while maintaining large permeance, which always appears to be a trade-off. The specific application of membranes depends on the pore sizes. Membranes with nominal pore sizes larger than 0.1 μm (or a M_w cut-off > 5000 kDa) are typically used in microfiltration for particles, large bacteria, blood cells, and yeasts. Ultrafiltration membranes possess nominal pore sizes ranging from 2 to 100 nm (or a M_w cut-off of 5–5000 kDa), and are effective for the separation of viruses, albumin proteins, and colloidal solids. Membranes with nominal pore sizes of 1–2 nm are often classified as nanofiltration membranes, and are used for separating synthetic dyes, sugars, and molecules larger than 5 kDa. The pore sizes of reverse osmosis (RO) membranes are generally smaller than 1 nm, leading to the effective removal

* Corresponding author.
E-mail address: kkg@mit.edu (K.K. Gleason).

https://doi.org/10.1016/j.eng.2020.05.002

of aqueous salts and small organic molecules (< 100 Da) [3]. Membranes with ultramicropores (pore sizes < 0.7 nm) are useful for gas separation, pervaporation, and vapor permeation [4,5].

Although this fact is often overlooked, common fabrication methods for membrane materials involve a wide variety of organic solvents, most of which are not environmentally benign. Solvent-less synthetic methods offer greener solutions for membrane fabrication. In recent years, vapor-phase approaches have been reported for synthesizing membrane materials. Ultrathin selective layers directly deposited on membrane substrates and precise pore engineering in membrane structures (Fig. 1) have enabled many sustainable separation processes such as gas separation, nanofiltration, desalination, and water/oil separation. This perspective covers the recent development of solvent-less deposition processes for advanced membrane materials.

2. Initiated chemical vapor deposition for membrane surface modification and fabrication

The initiated chemical vapor deposition (iCVD) polymerization method holds great promise for developing improved membranes for a multitude of separation processes (Table 1 and Fig. 2) [6–26]. Ultrathin free-standing membranes have been fabricated by means of iCVD alone (Fig. 2(a)) for envisioned biomedical applications and biomedical microelectromechanical systems (bioMEMS) applications, such as the fabrication of a lung-assist device [8]. However, iCVD is more commonly utilized to modify base membrane supports. This enables independent optimization of the surface and bulk properties. As a vapor-phase method, iCVD eliminates the potential for solvent-induced swelling or damage to the base membrane. In addition, iCVD allows surface tension effects, such as dewetting, to be avoided, making the formation of pinhole-free surface modification layers of uniform thickness possible, even over complex porous geometries.

In iCVD [27], monomers and a free-radical initiator are introduced as vapors into a reactor held at modest vacuum (~0.1 to ~1 Torr, 1 Torr ≈ 133.3224 Pa). The array of wires inside the reactor is heated to 250–300 °C, which decomposes the initiator but not the monomer. The reactive species adsorb and polymerize on a cooled surface, typically held at around 25 °C. The low temperature of the growth surface is ideal for avoiding damage to fragile substrates, such as porous polymeric membranes.

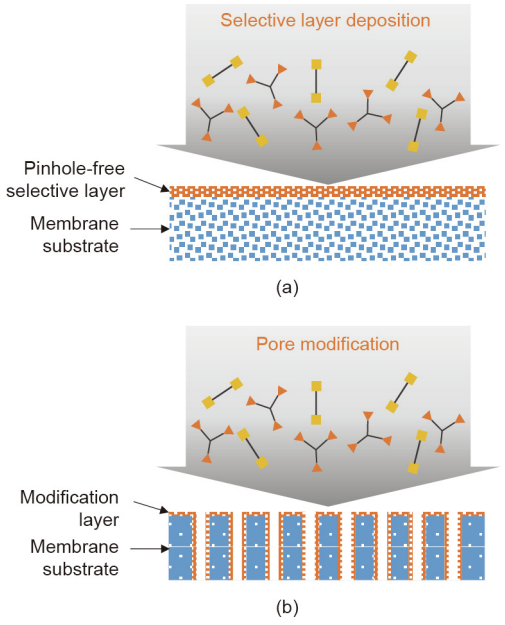

Fig. 1. Schematic illustration of solvent-less vapor-phase deposition for the fabrication of a thin-film composite membrane comprised of (a) a blanket layer over a porous support and (b) a conformal coverage penetrating into interior pore surfaces.

The large library of iCVD monomers enables the synthesis of a diverse array of homopolymers and copolymers (see Table 1 for examples). Selection of specific iCVD polymers is a key design parameter for achieving fouling-resistant surfaces, stimuli-responsive layers, and highly efficient separations based on specific molecular interactions. The organic functional groups displayed by iCVD polymers include both simple moieties, such as hydroxyl (–OH), carboxyl (–COOH), and amine ($–NH_2$) groups, and more complex structures, such as zwitterionic moieties.

For membrane applications, copolymerization commonly utilizes crosslinking monomers containing two or more vinyl bonds. With the iCVD approach, crosslinking occurs simultaneously with polymerization and thin-film formation. There is no need for any post-deposition annealing or ultraviolet (UV)-curing steps to achieve crosslinking by iCVD. The crosslinker imparts durability and low surface roughness to the resulting iCVD film. Using the iCVD vapor-phase approach permits the copolymerization of monomers that do not have a common solvent. Indeed, mixing the vapors of a fluorine-containing monomer with a hydrogel-forming monomer enabled random iCVD copolymerization, leading to the formation of an amphiphilic surface resistant to protein fouling [28] and proton-exchange membranes for fuel cells [20].

Novel membranes result from combining iCVD layers with a variety of membrane supports (Table 1). Demonstrated iCVD compositions can impart hydrophobic, hydrophilic, responsive, or fouling resistance to membranes as either blanket layers (Fig. 1(a)) or conformal coatings (Fig. 1(b)).

A blanket anti-biofouling iCVD layer robustly grafted to an underlying commercial RO desalination membrane (Fig. 2(b)) can reduce the frequency of costly shutdowns for membrane cleaning [25]. iCVD copolymer films exhibit excellent antifouling performance, mainly due to two reasons: First, iCVD copolymers and zwitterionic coatings can generate a hydrophilic surface/hydration layer to reduce protein and bacteria adsorption [10,17]; second, iCVD random copolymers possess compositional heterogeneities in the same dimension as the foulant, resulting in thermodynamically unfavorable interaction between the biofoulant and the surface [28]. As ultrathin films (< 30 nm thick), the antifouling layers have a limited impact on water permeability. Combining blanket iCVD layers with an anodized aluminum oxide (AAO) support results in novel composite membranes in which the iCVD hydrogel films provide permselectivity [9].

Applying iCVD conformally, rather than as a blanket layer, modifies the surface chemistry over the entire pore architecture of the base membrane, and can systematically decrease pore diameter (Fig. 1(b)). Covering the interiors of the cylindrical nanopores of a base track-etched polycarbonate with conformal hydrophobic iCVD coatings altered the surface chemistry inside the pores and narrowed their mean diameter down from 50 to < 5 nm. At this small final diameter, the separation of similarly sized molecules was achieved based on the difference in their hydrophobicity [12]. Conformally coating AAO membranes with a responsive iCVD layer create a smart membrane that switches on and off the passage of protein [14]. In the collapsed state, the iCVD layer has a thickness of about 30 nm (Fig. 2(c)) and the pore is open. Changing the temperature causes the iCVD layer to swell with water, effectively closing off the pores (Fig. 2(d)). Smart membranes have also been fabricated with pH-responsive iCVD layers [13]. Figs. 2(e) and (f) demonstrate that tortuous pore architectures can also be conformally modified by iCVD [18] to create membranes for oil/water separation.

Table 1
Selected examples of membranes fabricated utilizing iCVD.

iCVD layer composition and structure	Sacrificial layer/base membrane	Key properties	Envisioned utility	Ref.
Free-standing nanoporous and microporous iCVD membranes				
Poly(*N*-isopropylacrylamide), ~450 nm thick, nanoporous	Ionic liquid[b]	Smart/responsive	Temperature-responsive hydrophilicity for biomedical applications	[6]
Poly(ethylene glycol diacrylate[a]), ~95 μm thick, microporous	Silicone oil[b]	Ultrathin and porous	Tissue engineering, electrolyte membranes	[7]
Poly(*n*-butyl acrylate), ~1 to 5 μm thick, nanoporous	Spun-cast poly(acrylic acid)[b]	Ultrathin and porous	Biocompatible membrane for gas exchange, integrated into a microfluidic lung-assist device	[8]
Poly(hydroxyethylmethacrylate-*co*-ethylene glycol dimethacrylate[a]), ~1 μm thick, nanoporous	Spun-cast poly(acrylic acid)[b]	Smart/responsive permselective layer	Swellable iCVD hydrogel layers with mesh sizes ~0.57–0.65 nm for size and polarity base separation of small molecules including dyes	[9]
Thin-film composite membranes with pinhole-free iCVD-selective blanket layers				
Poly(4-vinylpyridine-*co*-divinylbenzene[a]), surface functionalized with 1,3-propanesultone, ~30 nm thick, grafted	Commercial RO membrane[c]	Fouling resistant	Zwitterionic anti-biofouling protection for water desalination, resistant to attack by chlorine, and maintains high water permeation	[10]
Poly(maleic anhydride-*co*-dimethylacrylamide-*co*-diethylene glycol divinyl ether[a]), ~ 150 nm thick, grafted	Anodized aluminum oxide[c]	Smart/responsive	Asymmetric membrane for size-selective separation of small molecules and proteins with a pH-responsive iCVD hydrogel-selective layer (pore size 3.2 nm at pH 7)	[11]
Conformal iCVD surface modification of cylindrical pores				
Poly(1*H*,1*H*,2*H*,2*H*-perfluorodecyl acrylate)/poly(divinyl benzene[a]) bilayers	Track-etched polycarbonate membranes[c], ~50 nm pore size	Hydrophobic	Fabrication of hydrophobic, cylindrical nanopores with diameters as low as 5 nm for hydrophobicity-based separation of molecules of similar size	[12]
Poly(methacrylic acid-*co*-ethylene glycol dimethyacrlate[a]), ~6 nm thick at pH 3, swelling to ~17 nm at pH 9	Anodized aluminum oxide[c], ~118 nm pore size	Smart/responsive	Smart membrane with pH-controllable diameter of cylindrical pores for switchable permeation control	[13]
Poly(*N*,*N*-dimethylaminoethyl methacrylate-*co*-ethylene glycol diacrylate[a]), ~35 to 90 nm thick	Track-etched polycarbonate membranes[c], ~50 nm pore size	Smart/responsive	Smart membrane with thermo-responsive nanovalves for switchable on–off control of protein permeation using 15-fold swelling ratio of the iCVD hydrogel	[14]
Other conformal iCVD surface modification				
Poly(1*H*,1*H*,2*H*,2*H*-perfluorodecyl acrylate), ~70 nm thick	Poly(caprolactone) electrospun fiber mats[c], beaded and bead-free fibers, with diameters ranging from 600 to 2200 nm	Hydrophobic	Membranes that are super-hydrophobic, with stable static contact angles with water of up to 175° and having high oleophobicity (grade 8 oil repellency)	[15]
Poly(divinyl benzene), ~10 nm thick	Commercial nylon phase inversion membranes[c], ~200 nm pore size	Hydrophobic	Hydrophobic membranes that are free of fluorine for use in the membrane desalination of water	[16]
Poly(*N*-vinyl pyrrolidone-*co*-ethylene glycol diacrylate[a]), grafted	Poly(vinylidene fluoride) microporous membrane[c], ~3 to 5 μm pore size	Fouling resistant	Durable membranes with tunable hydrophilicity and anti-biofouling properties	[17]
Poly(hydroxyethyl methacrylate-*co*-isocyanatoethyl methacrylate), ~70 nm thick, grafted	Poly(vinylidene fluoride) microporous membrane[c]	Cyano functionalization for adhesion of hydrogel coating to the substrate	Durable, high-flux, oil–water separation membranes	[18]
Poly[(2-dimethylamino)ethyl methacrylate-*co*-4-vinyl benzyl chloride]	Stainless-steel mesh[c], 38 μm openings	Crosslinked ionic, permselective layers	Crosslinked ionic polymers via a Menshutkin nucleophilic substitution reaction; durable, high-flux, oil–water separation membranes	[19]
Poly(1*H*,1*H*,2*H*,2*H*-perfluorodecyl methacrylate-*co*-methylacrylic acid), ~1 μm thick	Commercial microporous polyethylene membrane[c], ~0.5 μm pore diameter	Proton conductivity	Proton-exchange membrane for a miniaturized fuel cell	[20]
Poly(2-methylaminomethyl styrene)	Stainless-steel mesh filter[c], ~38 μm openings	Amino functionalization for selective binding	Direct nucleic acid extraction for gene expression analysis	[21]
Poly(1*H*,1*H*,2*H*,2*H*-perfluorodecyl methacrylate)	Stainless-steel mesh filter[c], ~38 μm openings	Hydrophobic	Separation of microalgal lipids from biomass for biofuel production	[22]
Poly(1*H*,1*H*,2*H*,2*H*-perfluorodecyl methacrylate)	Commercial macroporous polyester membrane[c]	One side hydrophobic, the other side fouling resistant	Hydrogel-functionalized Janus membrane for skin regeneration and wound healing	[23]

[a] Signifies a crosslinking monomeric unit for added durability.
[b] Sacrificial layer.
[c] Base membrane.

The macroscale openings of steel mesh supports provide high permeability. Conformal hydrophilic zwitterionic iCVD coatings encasing the mesh structure allow the rapid passage of water through the openings in the mesh, leaving oil behind [29]. Using the inverse strategy, hydrophobic iCVD-coated meshes allow the rapid passage of algae lipids, which are desired as a biofuel, from water-based emulsions [22]. Nucleic acid separation has also been demonstrated with iCVD-coated steel meshes [21].

For water desalination by means of membrane distillation, only water vapor should pass through the pores, causing brine to concentrate on one side of the membrane (Fig. 3(a) [16]). Optimal operation requires a narrower pore size distribution than is

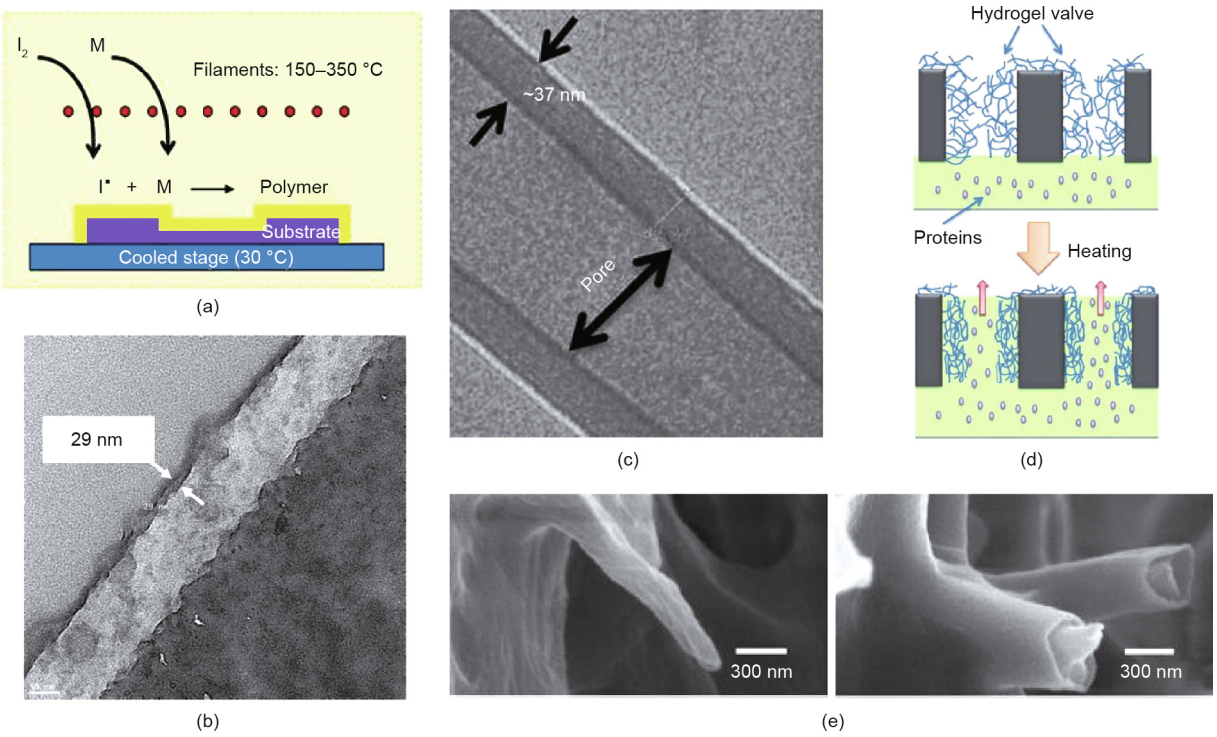

Fig. 2. (a) Schematic of iCVD polymer thin-film growth from monomer and initiator vapors [24]; (b) cross-sectional transmission electron microscopy (TEM) image for an ultrathin blanket iCVD antifouling layer on a commercial RO membrane [25]; (c) conformal iCVD coating on the interior of the cylindrical pore wall [14]; (d) schematic of the on–off switching of a nanovalve fabricated with a conformal iCVD hydrogel layer [14]; (e) the complex porous architecture of a poly(vinylidene fluoride) membrane before (left) and after (right) conformal iCVD surface modification [17].

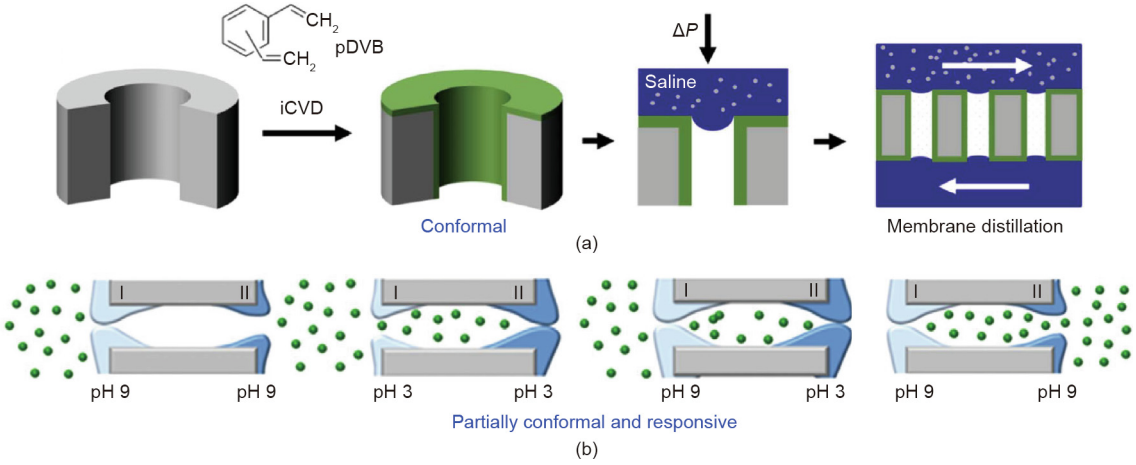

Fig. 3. Separation processes using novel membranes fabricated via iCVD. (a) A fluorine-free hydrophobic conformal coating permits only water vapor from the saline to pass through the pore [16]; (b) keyhole-shaped pores from partially conformal iCVD pH-responsive layers produce the directional transport of protein as pH is varied on each side of the smart membrane [33]. pDVB: poly(divinylbenzene).

typically available with commercial hydrophobic membranes. Nylon membranes can provide the desired narrow pore-size distribution, but are hydrophilic. However, a nylon membrane can be made hydrophobic by conformal iCVD hydrophobic surface modification [16]. Other types of membrane substrates have also been iCVD surface modified for potential application in membrane distillation [30,31]. Using a blanket hydrophobic layer on one side of the base membrane with a blanket hydrophilic layer on the other produces Janus membranes [23] and Janus films [32], which are used for oil/water separation, wound healing, and other applications. Fig. 3(b) shows a responsive Janus membrane for the directional transport of protein [33]. On each side of the membrane, a pH-responsive iCVD layer was coated in a partially conformal manner at a P/P_{sat} of about 0.3 to create keyhole-shaped pores. These pores open and close as gates when the pH is switched in succession, in order to produce unidirectional mass transport.

The consumption rate of the monomer to form films relative to the monomer's diffusion rate, as quantified by the Thiele modulus (θ), is key to determining the final architecture of the iCVD modified porous media [34]. The value of θ is proportional to pore length squared and inversely proportional to pore radius. The precise equation for θ depends on the underlying kinetic mechanism of the deposition process.

For $\theta \gg 1$, iCVD polymerization is rapid compared to the rate at which monomer vapor diffuses into the pores. Hence a blanket iCVD layer forms over the top surface of the membrane. In order to function as the selective layer of thin film composite membrane, the blanket layer must be free of pinhole defects. Additionally, the blanket layer must be ultrathin in order to maintain high permeation rates across the composite structure. Optimization to achieve the sub-1 nm roughness levels enables ultrathin pinhole free iCVD layers to form. In contrast, surface tension effects make defect-free ultrathin layers difficult to form by liquid-based methods.

For $\theta \ll 1$, the monomer is able to rapidly diffuse down the length of the pore before reacting, allowing all of the internal pore wall surfaces to be uniformly covered. Conformal deposition on cylindrical pores causes their diameter to shrink uniformly down their length. Under optimized conditions, iCVD has achieved conformal coverage of cylindrical pores 4000× longer than their diameter. Conformal iCVD coverage is also possible on tortuous pore geometries. In contrast, the ability to achieve conformal coverage by liquid-based coating methods is often limited by the effects of surface tension. For $\theta \ll 1$, the iCVD layers formed at the pore mouth will be thicker than in the interior of the pore, resulting in bottleneck-shaped pores.

Since the iCVD layer starts at the surface of the substrate, it is possible to engineer the formation of covalent bonds across the interface as the iCVD process commences. The goal is to promote the functional groups present on the surface of the substrates to undergo chemical reactions with complementary functional groups in the iCVD film. The grafting reduces the probability of the surface modification layer delaminating, and is particularly valuable for enhancing the durability of thin-film composite membranes. The geometry of conformal surface modification has reduced probability to fail by delamination.

3. Initiated plasma-enhanced chemical vapor deposition for porphyrinic metal–organic covalent network membranes

Their microporous structure and narrow pore-size distribution make porphyrin polymers attractive for the adsorption, separation, and sensing of gases. While a variety of porphyrin-based metal–organic frameworks (MOFs) and covalent organic frameworks (COFs) have been reported, it is still challenging to fabricate pinhole-free large-area membranes with nanoscale thickness. Taking advantage of the solvent-less initiated plasma-enhanced chemical vapor deposition (iPECVD) process, Boscher et al. [35,36] and Wang et al. [37] developed a series of ultrathin (20–100 nm) porphyrin-based metal–organic covalent networks (MOCNs). This iPECVD process has been shown to be a scalable, facile approach to synthesize free-radical polymerized porphyrin networks in a single step over a large substrate area (175 cm^2). In addition, the soft radio frequency (RF) plasma employed in the iPECVD process allows the use of delicate substrate materials such as the porous polymer support for MOCN membranes.

In a typical iPECVD process (Fig. 4(a)), low-power capacitive coupled Ar plasma cleaves the O–O bonds in *tert*-butyl peroxide

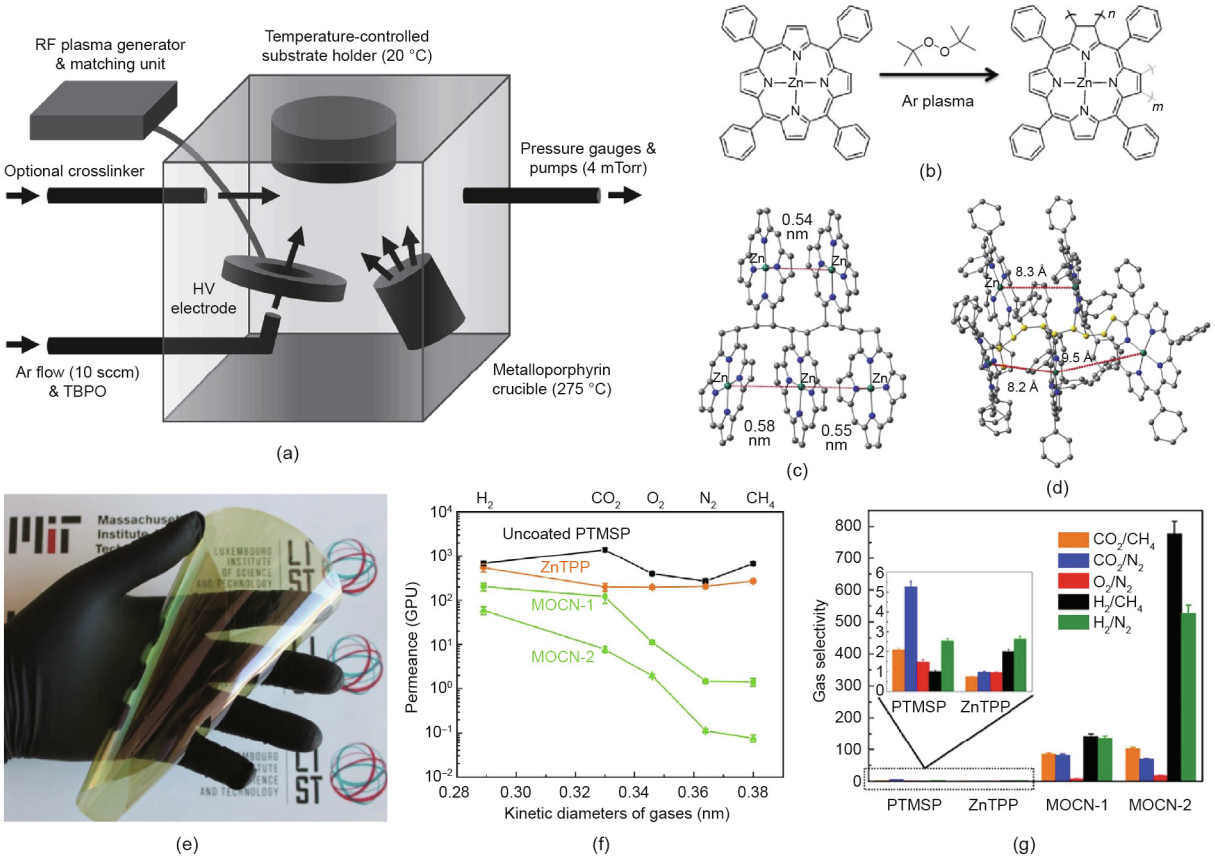

Fig. 4. (a) Illustration of the iPECVD reactor for the solvent-less synthesis of MOCN membranes [36]. (b) Reaction schematic for forming poly(Zn(II) *meso*-tetraphenylchlorin) (poly(ZnTPC)) MOCN via iPECVD free-radical polymerization. (c, d) Density functional theory (DFT)-optimized pentamer structure of $[ZnTPC]_5$ (hydrogen omitted; color code: grey for carbon, blue for nitrogen, green for zinc) [35,37]. Phenyl rings were truncated for DFT calculation in (c), while (d) shows the full structure of the $[ZnTPC]_5$ pentamer (carbon atoms in the polymer backbone are color-coded yellow). (e) Photo of a large-area flexible poly(1-trimethylsilyl-1-propyne) (PTMSP) membrane coated with an iPECVD MOCN selective skin layer. (f, g) Gas-separation performance of an uncoated PTMSP membrane and of PTMSP membranes coated with evaporated Zn(II) *meso*-tetraphenylporphyrin (ZnTPP) film and iPECVD MOCN films. Film thickness is 47 nm for MOCN-1 and 67 nm for MOCN-2 [35]. HV: high voltage; sccm: standard cubic centimeter per minute; GPU: gas permeation unit.

(TBPO) and generates free radicals. Metalloporphyrin monomers are evaporated from a heated crucible (275 °C) and polymerize on the substrate surface with the presence of *tert*-butoxy radicals. Optional crosslinkers such as divinylbenzene (DVB) can also be delivered into the vacuum chamber and copolymerize with the metalloporphyrin, offering additional tunability in the design and synthesis of MOCN structures.

Spectroscopic analyses reveal that Zn(II) *meso*-tetraphenylporphyrin (ZnTPP) is reduced to Zn(II) *meso*-tetraphenylchlorin (ZnTPC) during the iPECVD process, indicating that the free-radical polymerization occurs at the *exo*-pyrrole double bonds (Fig. 4(b)). Less pronounced π–π stacking of the porphyrin structures was also found in iPECVD MOCN from the spectral results. As illustrated in Figs. 4(c) and (d), the molecular structures of $[ZnTPC]_5$ pentamers optimized via density functional theory (DFT) show the pore size and geometry. The truncated model shows an average Zn–Zn distance of about 0.56 nm, while the full model reveals the Zn–Zn distance to be about 0.87 nm with consideration of all phenyl rings at *meso*-positions [37]. The actual pore size of the iPECVD MOCN film, which was determined using ellipsometric porosimetry, is as low as 0.4 nm, which is in the perfect range for separations via molecular sieving.

Large-area MOCN membranes have been deposited on poly(1-trimethylsilyl-1-propyne) (PTMSP) substrates (Fig. 4(e)) [35]. Effective molecular sieving of MOCN membranes suppresses the permeance of gases with a large kinetic diameter (i.e., CH_4 and N_2), while the high flux of smaller gas molecules is maintained (Fig. 4(f)). Single gas permeation tests reveal that the separation selectivity of uncoated PTMSP and thermal-evaporated ZnTPP membranes is generally below 5, regardless of the gas pairs. The low selectivity of evaporated ZnTPP membranes is due to major defects being present in the ZnTPP layer [35]. This metalloporphyrin tends to crystallize during thermal evaporation, so it may leave a significant number of defects at the grain boundaries in ultrathin polycrystalline films. In contrast, the separation selectivity for H_2/CH_4 and H_2/N_2 gas pairs reaches over 130 with a defect-free iPECVD poly(ZnTPC) membrane, while H_2 permeance maintains over 200 gas permeation units (GPU). Excellent separation performance has also been obtained for CO_2/CH_4 and CO_2/N_2. Separation of these gas pairs has significant industrial implication in H_2 recovery, pre-combustion CH_4 purification, and CO_2 capture from flue gas.

Boscher et al. [36] further expanded the iPECVD chemistry for MOCNs by introducing multi-vinyl crosslinkers during the free-radical polymerization of metalloporphyrins. Separation selectivity for CO_2/CH_4 over 150 has been achieved with poly(DVB-*co*-ZnTPC) membranes. Wang et al. [37] investigated the role of the center metal ion of porphyrinic MOCNs in gas separation performance. Poly(*meso*-tetraphenylchlorin), poly(Mn(III) (*meso*-tetraphenylchlorin) chloride), and poly(Co(II) *meso*-tetraphenylchlorin) membranes have been synthesized using the iPECVD process and compared with poly(ZnTPC). DFT calculations show that the center metal ion does change the packing structure of the MOCNs. Consequently, high performance for gas separation has been demonstrated for all four MOCN membranes.

4. The solvent-less vapor deposition followed by *in situ* polymerization process for polyimide membranes

Polyimide (e.g., Matrimid®) is commonly used for gas separation membranes, and has been widely studied in the past [38]. Developed by the Lawrence Livermore National Laboratory (LLNL), the solvent-less vapor deposition followed by *in situ* polymerization (SLIP) process is capable of forming polyimide thin films on substrate membranes [39,40]. During the SLIP process, a dianhydride (e.g., pyromellitic dianhydride (PMDA) and 5,5′-[2,2,2,-trofluoro-1-(trifluoromethyl) ethylidene] bis-1,3-isobenzofuranedione (6FDA)) and a diamine such as oxydianiline (ODA) are evaporated separately and delivered into the vacuum chamber simultaneously (Fig. 5(a)). After passing through a mixing nozzle, a polyamic acid thin film is deposited onto the substrate surface. A final *in situ* imidization step is required to convert the polyamic acid into polyimide for the thin-film composite membrane (Fig. 5(b)). The growth rate was found to be 11 $nm \cdot s^{-1}$ for PMDA-ODA and 2.5 $nm \cdot s^{-1}$ for 6FDA-ODA [40]. This deposition rate is promising for high-throughput manufacturing if the SLIP process can be scaled up.

The use of delicate polymer substrates actually limits the temperature that can be used for the thermal imidization reaction in SLIP. Spadaccini et al. [40] reported lowering the imidization temperature from 300 to 180 °C in order to adopt the process for the amorphous fluoropolymer (perfluorodioxole) substrate. Although complete imidization has been achieved for PMDA-ODA, the limited degree of imidization for 6FDA-ODA makes this SLIP polymer unqualified for gas separation. The PMDA-ODA membrane fabricated via the SLIP process enables a CO_2 permeance of 79 GPU (calculated from Ref. [39]) with a CO_2/N_2 selectivity of 24.5 [39].

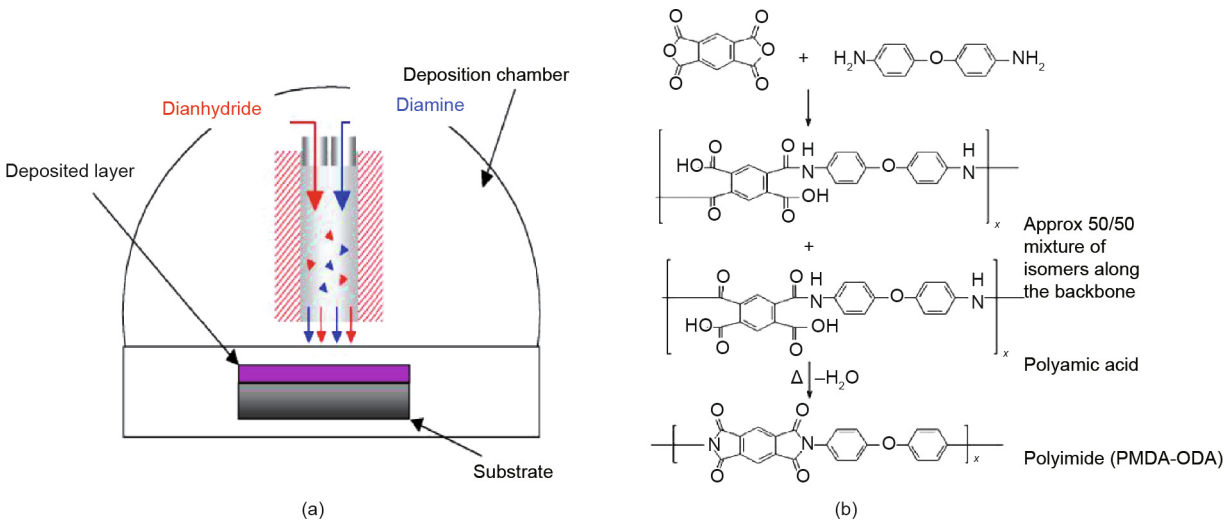

Fig. 5. (a) Reactor scheme for the SLIP process for polyimide membranes; (b) reaction route for the synthesis of polyimide (PMDA-ODA) [40].

Further optimization of the SLIP process is needed to develop new polyimide membranes with enhanced separation performance.

5. Atomic/molecular layer deposition for MOF membranes

Atomic layer deposition (ALD) is a vapor-phase deposition process that is widely used in semiconductor manufacturing. Due to the self-limiting effect of precursor chemisorption, ALD is powerful in its precise control of film thickness at a sub-nanometer scale and its exceptional conformality in high-aspect-ratio nano-structures [41]. In addition, ALD processes have been developed for a wide variety of materials including metals, oxides, nitrides, sulfides, and many other compounds [42]. These advantages of ALD have given rise to extensive research efforts in tuning membrane pore structures for separation applications [43–47]. Fig. 6(a) depicts a typical ALD process involving the cycling processes of sequential precursor doses and inert purge steps [48]. Taking ALD Al_2O_3 as an example, trimethylaluminum (TMA) reacts with surface –OH groups in the first half reaction and creates a $–CH_3$ terminated surface. In the second half reaction of the ALD cycle, H_2O vapor reacts with the $–CH_3$ terminated surface via ligand exchange, thus changing the surface into –OH groups again. Purge steps between the half reactions ensure the complete removal of unreacted precursors and byproduct CH_4. Monolayers of Al_2O_3 are added sequentially onto the surface by repeating these process cycles.

Molecular layer deposition (MLD) is analogous to ALD and is based on self-saturating surface reactions in repeating cycles

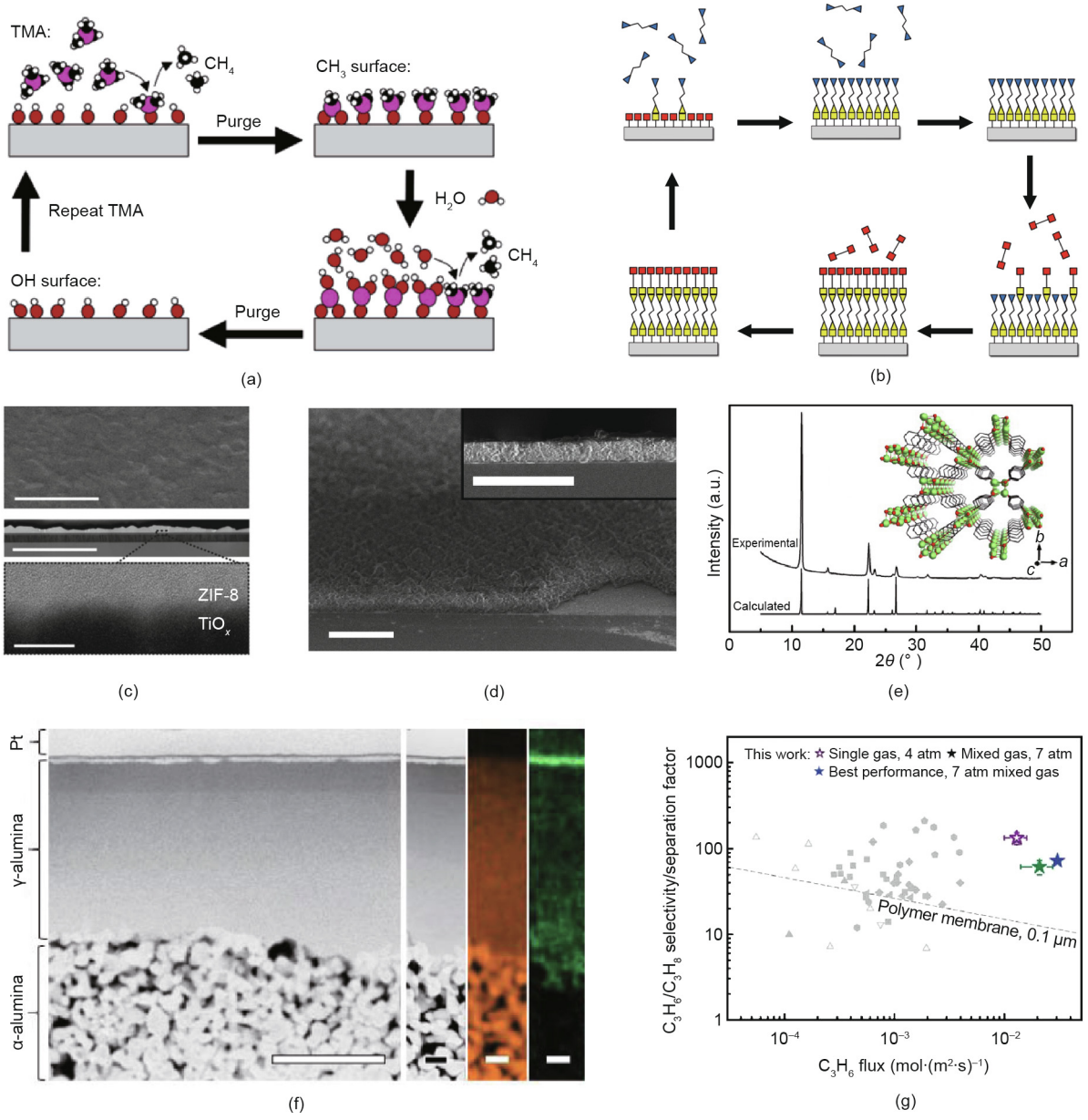

Fig. 6. Process scheme for (a) a typical ALD process [48] and (b) an MLD process [49]. (c) Scanning electron microscope (SEM) and cross-sectional TEM images of zeolitic imidazolate framework (ZIF)-8 thin film deposited on a TiO_x substrate via the ALD-chemical vapor deposition (CVD) process [61]. (Scale bar in top and middle images: 2 μm; scale bar in the inset: 20 nm.) (d) SEM images of UiO-66 thin film synthesized through modified ALD [63]. (Scale bar represents 2 μm.) (e) Experimental and calculated X-ray diffraction (XRD) patterns of $Li_2[p\text{-}C_6H_4O_2]$ thin film deposited via the ALD/MLD process; inset shows the crystal structure of $Li_2[p\text{-}C_6H_4O_2]$ [68]. (f) Cross-sectional annular dark-field scanning transmission electron microscopy (ADF-STEM) imaging with energy dispersive X-ray spectroscopy (EDX) mapping for Al (orange) and Zn (green) for a ZIF-filled γ-alumina membrane on top of an α-alumina substrate [70]. (The large scale bar represents 2 μm; the small scale bar represents 400 nm.) (g) Separation performance for C_3H_6/C_3H_8 using the ZIF-filled alumina membrane [70]. TMA: trimethylaluminum. 1 atm = 101 325 Pa.

(Fig. 6(b) [49]). This solvent-less vacuum deposition can be used to create organic polymer thin films including polyamide, polyimide, copolymers of polyimide–polyamide, polyurethane, and polyurea. In addition, using organometallic precursors and bifunctional ligands such as ethylene glycol, diamines, and dithiols, MLD can be employed to deposit "metalcone" hybrid organic–inorganic materials [49]. Similar to ALD, MLD exhibits great advantages in tuning pore size and internal functionality for membrane structures [50,51].

The use of ALD and MLD for membrane fabrication has been recently reviewed by Weber et al. [4]. Here, we simply highlight recent research efforts in synthesizing MOF thin films using ALD and MLD. Assembled from metal-containing secondary building units and organic ligands, MOFs are characterized by ordered pore structures, a large surface area, and amenability for post-synthetic modification. These characteristics result in the exceptional gas separation performance of MOF membranes, which exceeds Robeson's upper bound defined for traditional membrane materials [52]. The motivation for developing vapor-phase deposition methods to prepare MOF membranes is to obtain ultrathin MOF skin layers with a high mass-transfer flux, which is very challenging for traditional solvothermal synthesis, and to avoid the use of organic solvent so that post-synthetic activation processes are no longer necessary.

The development of ALD/MLD processes for MOF thin films includes two main thrusts. One of these thrusts is based on the facile conversion from a metal oxide precursor to the MOF structures. Previous research has found that ALD metal oxides can act as interfacial layers for tuning MOF nucleation [53–55], form hydroxyl double salt intermediates and convert into MOFs [56–58], or react directly with organic linkers to generate MOF films [59–61]. For example, ALD ZnO can react with 2-methylimidazole vapor to form zeolitic imidazolate framework (ZIF)-8 thin films in an ALD-chemical vapor deposition (CVD) process (Fig. 6(c)) [61]. The other thrust is to directly adapt the ALD/MLD process to synthesize MOF structures. Thus far, MOF thin films that can be directly deposited via ALD/MLD include MOF-5 [62], UiO-66 (Fig. 6(d)) [63], UiO-66-NH_2 [64], Cu-benzenedicarboxylic (BDC) [65], Ca-BDC [66], Fe-BDC [67], and $Li_2[p\text{-}C_6H_4O_2]$ (Fig. 6(e)) [68]. Ongoing research aims to further explore ALD/MLD chemistry in order to expand these processes for MOF thin films.

Taking advantage of the vapor-phase conversion from ZnO to ZIF-8, Ma et al. [70] recently reported a membrane fabrication method using ALD ZnO and subsequent ligand vapor treatment. This MOF was chosen because it possesses aperture (pore window) sizes of about 3.4 Å, which is in the appropriate range for the kinetic separation of propylene and propane [69]. A ZIF-filled γ-alumina membrane on top of an α-alumina substrate (Fig. 6(f)) enables a C_3H_6/C_3H_8 selectivity over 100 with a C_3H_6 permeance as high as 3.81×10^{-8} mol·(m^2·s·Pa)$^{-1}$ (or 114 GPU) [70]. This excellent gas separation performance is among the best data reported for ZIF-8 and ZIF-67 membranes, and surpasses the Robeson's upper bound for C_3H_6/C_3H_8 (Fig. 6(g)) [70], which demonstrates the great promise of ALD processes for making high-performance MOF separation membranes.

6. Conclusion and future outlook

Solvent-less vapor-phase deposition methods have shown great promise in precisely modifying the nanoscale pores in membranes as well as in synthesizing ultrathin selective layers for thin-film composite membrane structures. These membranes have been applied to a wide variety of sustainable separation processes including gas separation, water filtration, oil/water separation, membrane distillation, separation of biomolecules, antifouling RO membranes, and proton-exchange membranes. In addition, membranes modified or fabricated using solvent-less vapor-phase techniques have enabled new applications in catalytic membrane reactors and biomedical sensors and devices. Table 2 summarizes the features and membrane applications of these vacuum deposition approaches used in membrane fabrication and modification. It is worth noting that these advanced synthesis methods cover a wide variety of materials ranging from organic polymers to inorganic materials. Furthermore, inorganic–organic hybrid materials such as metalcones, MOFs, and MOCNs have been successfully grown using these solvent-less vapor-phase approaches. The wide range of materials available for vacuum deposition processes offers great flexibility for the design and fabrication of membranes.

Most of the processes discussed here can be performed at low chamber/substrate temperatures, enabling the use of delicate substrate materials including polymers with a low glass transition temperature and melting point. Since a cooling stage is used in the iCVD and iPECVD processes, the substrate materials can be kept at room temperature or even lower temperatures. ALD and MLD process conditions usually depend on the materials to grow in

Table 2
Summary of solvent-less vapor-phase deposition processes for membrane fabrication.

Process	Materials grown in solvent-less vapor-phase process	Process temperature	Conformality	Reactor scalability	Membrane applications reported
iCVD	Polymers of fluorocarbon, organosilicon, acrylate, methacrylate, styrene, and other vinyl monomers	Substrate temperature: −10–100 °C	Excellent	Industry-scale reactors already available	Oil/water separation, membrane distillation, water filtration, antifouling RO membranes, ion-exchange membranes, separation of biomolecules, artificial lung, and other biomedical and bioMEMS applications
iPECVD	Polymers of common iCVD monomers, metalloporphyrin polymers, and MOCNs	Substrate temperature: 20–100 °C	Good	Scalable	Gas separation
SLIP	Polyimides	180–300 °C	Not demonstrated	Not demonstrated	Gas separation
ALD	Inorganic materials including pure elements, oxides, nitrides, sulfides, perovskites, and MOFs	Vary with materials. Typical temperature: < 350 °C	Excellent	Industry-scale reactors already available	Gas separation, water filtration, biosensing, catalysis, microfluidics, and osmotic energy
MLD	Inorganic–organic hybrid materials ("metalcones"), polymers including polyamides, polyimides, polyurethanes, polyureas, polyazomethines, poly(3,4-ethylenedioxythiophene) (PEDOT)	Vary with materials. Typical temperature: room temperature to 200 °C	Excellent	Scalable	Water filtration, separation of biomolecules

order to achieve self-limiting growth in each cycle, while a great number of ALD and MLD processes are available for mild temperature conditions that can be easily applied for membranes. As mentioned above, the SLIP approach at low temperatures may affect the degree of imidization and, therefore, may affect the membrane properties. Careful selection of substrate materials may be required for the SLIP fabrication of asymmetric membranes.

Conformal deposition processes are highly desirable for precise modification of internal functionalities within pores and fine-tuning of pore dimensions. iCVD, ALD, and MLD have been demonstrated to produce excellent conformality in non-planar structures, such as nanoscale trenches with very large aspect ratios and tortuous pore structures. In iPECVD, the directionality of the plasma source affects the conformality of the deposited films. However, employing ultra-short plasma pulses and matching the plasma-off time with the lifetime of the free-radical polymerization have been reported to be effective means of generating good conformality for iPECVD polymer films [71,72]. The conformality of SLIP process has not been demonstrated.

The future development of these advanced manufacturing processes should focus on new membrane materials for enhanced separation performance, novel applications beyond separations and filtrations, and reactor scale-up for continuous high-throughput production.

New membrane materials enabling high separation selectivity and large permeance are always demanded for a variety of industrial separation processes. In addition to the small gas pairs commonly tested in research papers, including CO_2/CH_4, CO_2/N_2, O_2/N_2, H_2/CH_4, and H_2/N_2, new membrane materials fabricated via solvent-less vapor-phase approaches are expected to tackle more challenging and impactful separation problems, such as the separation of alkenes from alkanes, C6–C8 arenes from each other, and other realistic chemical mixtures [1]. Given that many emerging porous materials such as MOCNs, MOFs, COFs, and other covalent networks have been reported with appropriate pore sizes and affinity for specific chemical pairs, research efforts in this field should be directed to the development of novel solvent-less deposition methods for these advanced membrane materials.

In addition to exploring common membrane applications, research efforts are encouraged to explore novel applications in order to take full advantage of these advanced fabrication processes. Coupling membranes with catalysts could potentially achieve highly selective formation of chemical products while simplifying the traditional unit operations required for reaction conversion plus separation [73]. The wide variety of materials that can be deposited inside membrane pores via the abovementioned processes offers great opportunities for designing and synthesizing new membrane reactors. Applications of membranes beyond separations and filtrations also include use in biomedical devices such as artificial lungs [8] and biosensors [74], and in energy-storage devices such as fuel cells [20] and Li–air batteries [75]. Their solvent-less feature and their compatibility with device-fabrication procedures in glove boxes and cleanrooms make these vacuum deposition processes promising for integrating active membranes into device structures.

The scale of manufacturing is also key to mass production. Fortunately, many large-scale roll-to-roll reactors have been developed and commercialized for solvent-less vapor-phase processes such as iCVD, ALD, and MLD (Fig. 7). For example, Fig. 7(a) and

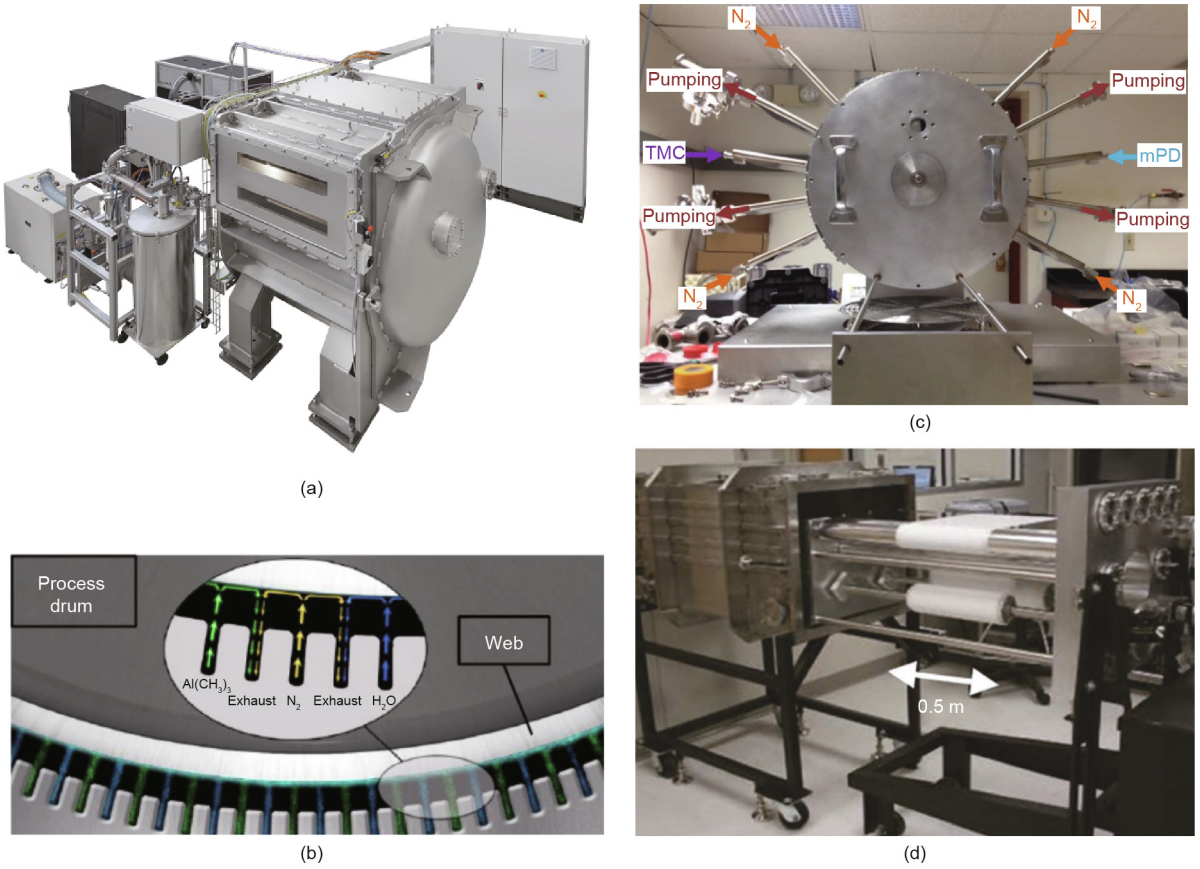

Fig. 7. (a, b) Spatial ALD in a commercial roll-to-roll ALD reactor for coatings on flexible substrates [76,77]; (c) a lab-scale spatial MLD reactor for large-area flexible substrates [78]; (d) a large-scale roll-to-roll iCVD reactor capable of surface modification for textiles and membranes [27]. TMC: trimesoyl chloride; mPD: *m*-phenylenediamine.

(b) [76,77] illustrate an industry-scale roll-to-roll ALD reactor with a spatially distributed precursor dose and inert gas purge outlets. These outlets enable continuous ALD deposition on the web surface as it moves along the process drum. Similar spatial design has also been reported in an effort to scale up the MLD process (Fig. 7(c)) [78]. Roll-to-roll iCVD reactors (Fig. 7(d)) [27] have been scaled up for 0.5 m wide textile and other soft materials, enabling continuous surface modification in high throughput. The design and scale-up of these vacuum reactors were motivated by the need for functional coatings and passivation layers on flexible substrates such as textiles and polymer films for soft electronics. By adapting a roll-to-roll reactor design, scaled-up reactors capable of handling large-area membrane substrates and forming high-performance membrane materials could significantly boost the advances in membrane production and make a real impact on the chemical industry.

Acknowledgements

Junjie Zhao acknowledges the start-up funding supported by Zhejiang University, the research grant from the State Key Laboratory of Chemical Engineering (SKL-ChE-19T04), and the funding support from the Institute of Zhejiang University–Quzhou (IZQ2019-KJ-011). Junjie Zhao also acknowledges the funding from the National Natural Science Foundation of China (21908194 and 21938011).

Compliance with ethics guidelines

Junjie Zhao and Karen K. Gleason declare that they have no conflict of interest or financial conflicts to disclose.

References

[1] Sholl DS, Lively RP. Seven chemical separations to change the world. Nature 2016;532(7600):435–7.
[2] Koros WJ, Zhang C. Materials for next-generation molecularly selective synthetic membranes. Nat Mater 2017;16(3):289–97.
[3] Singh R. Water and membrane treatment. In: Singh R, editor. Hybrid membrane systems for water purification. Amsterdam: Elsevier Science; 2006. p. 57–130.
[4] Weber M, Julbe A, Ayral A, Miele P, Bechelany M. Atomic layer deposition for membranes: basics, challenges, and opportunities. Chem Mater 2018;30(21):7368–90.
[5] Lepoitevin M, Ma T, Bechelany M, Janot JM, Balme S. Functionalization of single solid state nanopores to mimic biological ion channels: a review. Adv Colloid Interface Sci 2017;250:195–213.
[6] Frank-Finney RJ, Haller PD, Gupta M. Ultrathin free-standing polymer films deposited onto patterned ionic liquids and silicone oil. Macromolecules 2012;45(1):165–70.
[7] Bradley LC, Gupta M. Microstructured films formed on liquid substrates via initiated chemical vapor deposition of cross-linked polymers. Langmuir 2015;31(29):7999–8005.
[8] Sreenivasan R, Bassett EK, Hoganson DM, Vacanti JP, Gleason KK. Ultra-thin, gas permeable free-standing and composite membranes for microfluidic lung assist devices. Biomaterials 2011;32(16):3883–9.
[9] Tufani A, Ince GO. Permeability of small molecules through vapor deposited polymer membranes. J Appl Polym Sci 2015;132(34):42453.
[10] Yang R, Jang H, Stocker R, Gleason KK. Synergistic prevention of biofouling in seawater desalination by zwitterionic surfaces and low-level chlorination. Adv Mater 2014;26(11):1711–8.
[11] Tenhaeff WE, Gleason KK. Surface-tethered pH-responsive hydrogel thin films as size-selective layers on nanoporous asymmetric membranes. Chem Mater 2009;21(18):4323–31.
[12] Asatekin A, Gleason KK. Polymeric nanopore membranes for hydrophobicity-based separations by conformal initiated chemical vapor deposition. Nano Lett 2011;11(2):677–86.
[13] Tufani A, Ince GO. Smart membranes with pH-responsive control of macromolecule permeability. J Membr Sci 2017;537:255–62.
[14] Ye Y, Mao Y. Vapor-based synthesis of ultrathin hydrogel coatings for thermo-responsive nanovalves. J Mater Chem 2011;21(22):7946–52.
[15] Ma M, Gupta M, Li Z, Zhai L, Gleason KK, Cohen RE, et al. Decorated electrospun fibers exhibiting superhydrophobicity. Adv Mater 2007;19(2):255–9.
[16] Servi AT, Kharraz J, Klee D, Notarangelo K, Eyob B, Guillen-Burrieza E, et al. A systematic study of the impact of hydrophobicity on the wetting of MD membranes. J Membr Sci 2016;520:850–9.
[17] Sun M, Wu Q, Xu J, He F, Brown AP, Ye Y. Vapor-based grafting of crosslinked poly(*N*-vinyl pyrrolidone) coatings with tuned hydrophilicity and anti-biofouling properties. J Mater Chem B 2016;4(15):2669–78.
[18] Feng J, Sun M, Ye Y. Ultradurable underwater superoleophobic surfaces obtained by vapor-synthesized layered polymer nanocoatings for highly efficient oil–water separation. J Mater Chem A 2017;5(29):14990–5.
[19] Joo M, Shin J, Kim J, You JB, Yoo Y, Kwak MJ, et al. One-step synthesis of cross-linked ionic polymer thin films in vapor phase and its application to an oil/water separation membrane. J Am Chem Soc 2017;139(6):2329–37.
[20] Coclite AM, Lund P, Di Mundo R, Palumbo F. Novel hybrid fluoro-carboxylated copolymers deposited by initiated chemical vapor deposition as protonic membranes. Polymer 2013;54(1):24–30.
[21] You JB, Kim YT, Lee KG, Choi Y, Choi S, Kim CH, et al. Surface-modified mesh filter for direct nucleic acid extraction and its application to gene expression analysis. Adv Healthc Mater 2017;6(20):1700642.
[22] Kwak MJ, Yoo Y, Lee HS, Kim J, Yang JW, Han JI, et al. A simple, cost-efficient method to separate microalgal lipids from wet biomass using surface energy-modified membranes. ACS Appl Mater Interfaces 2016;8(1):600–8.
[23] An YH, Yu SJ, Kim IS, Kim SH, Moon JM, Kim SL, et al. Hydrogel functionalized Janus membrane for skin regeneration. Adv Healthc Mater 2017;6(5):1600795.
[24] Xu J, Gleason KK. Conformal polymeric thin films by low-temperature rapid initiated chemical vapor deposition (iCVD) using *tert*-butyl peroxybenzoate as an initiator. ACS Appl Mater Interfaces 2011;3(7):2410–6.
[25] Matin A. Enhancing the biofouling resistance of reverse osmosis membranes by a novel surface modification technique [dissertation]. Dhahran: King Fahd University of Petroleum and Minerals; 2012.
[26] Yang R. Membrane modification by CVD polymers. In: Gleason KK, editor. CVD polymers. Hoboken: John Wiley & Sons; 2015. p. 279–300.
[27] Coclite AM, Howden RM, Borrelli DC, Petruczok CD, Yang R, Yagüe JL, et al. 25th anniversary article: CVD polymers: a new paradigm for surface modification and device fabrication. Adv Mater 2013;25(38):5392–423.
[28] Baxamusa SH, Gleason KK. Random copolymer films with molecular-scale compositional heterogeneities that interfere with protein adsorption. Adv Funct Mater 2009;19(21):3489–96.
[29] Yang R, Moni P, Gleason KK. Ultrathin zwitterionic coatings for roughness-independent underwater superoleophobicity and gravity-driven oil–water separation. Adv Mater Interfaces 2015;2(2):1400489.
[30] Cai J, Liu X, Zhao Y, Guo F. Membrane desalination using surface fluorination treated electrospun polyacrylonitrile membranes with nonwoven structure and quasi-parallel fibrous structure. Desalination 2018;429:70–5.
[31] Cong S, Liu X, Guo F. Membrane distillation using surface modified multi-layer porous ceramics. Int J Heat Mass Transf 2019;129:764–72.
[32] Ye Y, Mao Y. Vapor-based synthesis and micropatterning of Janus thin films with distinct surface wettability and mechanical robustness. RSC Adv 2017;7(40):24569–75.
[33] Tufani A, Ozaydin Ince G. Protein gating by vapor deposited Janus membranes. J Membr Sci 2019;575:126–34.
[34] Ozaydin-Ince G, Coclite AM, Gleason KK. CVD of polymeric thin films: applications in sensors, biotechnology, microelectronics/organic electronics, microfluidics, MEMS, composites and membranes. Rep Prog Phys 2012;75(1):016501.
[35] Boscher ND, Wang M, Perrotta A, Heinze K, Creatore M, Gleason KK. Metal–organic covalent network chemical vapor deposition for gas separation. Adv Mater 2016;28(34):7479–85.
[36] Boscher ND, Wang M, Gleason KK. Chemical vapour deposition of metalloporphyrins: a simple route towards the preparation of gas separation membranes. J Mater Chem A 2016;4(46):18144–52.
[37] Wang M, Boscher ND, Heinze K, Gleason KK. Gas selective ultrathin organic covalent networks synthesized by iPECVD: does the central metal ion matter? Adv Funct Mater 2017;27(29):1606652.
[38] Wang M, Zhao J, Wang X, Liu A, Gleason KK. Recent progress on submicron gas-selective polymeric membranes. J Mater Chem A 2017;5(19):8860–86.
[39] O'Brien KC, Letts SA, Spadaccini CM, Morse JC, Buckley SR, Fischer LE, et al., inventors; Lawrence Livermore National Security LLC, assignee. Preparation of membranes using solvent-less vapor deposition followed by *in-situ* polymerization. United States patent US7754281B2. 2010 Jul 13.
[40] Spadaccini CM, Mukerjee EV, Letts SA, Maiti A, O'Brien KC. Ultrathin polymer membranes for high throughput CO_2 capture. Energy Procedia 2011;4:731–6.
[41] Parsons GN, George SM, Knez M. Progress and future directions for atomic layer deposition and ALD-based chemistry. MRS Bull 2011;36(11):865–71.
[42] Johnson RW, Hultqvist A, Bent SF. A brief review of atomic layer deposition: from fundamentals to applications. Mater Today 2014;17(5):236–46.
[43] Feng J, Xiong S, Wang Z, Cui Z, Sun SP, Wang Y. Atomic layer deposition of metal oxides on carbon nanotube fabrics for robust, hydrophilic ultrafiltration membranes. J Membr Sci 2018;550:246–53.
[44] Xiong S, Yang Y, Zhong Z, Wang Y. One-step synthesis of carbon-hybridized ZnO on polymeric foams by atomic layer deposition for efficient absorption of oils from water. Ind Eng Chem Res 2018;57(4):1269–76.
[45] Chen H, Wu S, Jia X, Xiong S, Wang Y. Atomic layer deposition fabricating of ceramic nanofiltration membranes for efficient separation of dyes from water. AIChE J 2018;64(7):2670–8.

[46] Feng J, Xiong S, Wang Y. Atomic layer deposition of TiO_2 on carbon-nanotube membranes for enhanced capacitive deionization. Sep Purif Technol 2019;213:70–7.
[47] Weber M, Kim JY, Lee JH, Kim JH, Iatsunskyi I, Coy E, et al. Highly efficient hydrogen sensors based on Pd nanoparticles supported on boron nitride coated ZnO nanowires. J Mater Chem A 2019;7(14):8107–16.
[48] Peng Q, Sun XY, Spagnola JC, Hyde GK, Spontak RJ, Parsons GN. Atomic layer deposition on electrospun polymer fibers as a direct route to Al_2O_3 microtubes with precise wall thickness control. Nano Lett 2007;7(3):719–22.
[49] George SM, Yoon B, Dameron AA. Surface chemistry for molecular layer deposition of organic and hybrid organic–inorganic polymers. Acc Chem Res 2009;42(4):498–508.
[50] Wu S, Wang Z, Xiong S, Wang Y. Tailoring TiO_2 membranes for nanofiltration and tight ultrafiltration by leveraging molecular layer deposition and crystallization. J Membr Sci 2019;578:149–55.
[51] Zhao Y, Sun X. Molecular layer deposition for energy conversion and storage. ACS Energy Lett 2018;3(4):899–914.
[52] Denny MS, Moreton JC, Benz L, Cohen SM. Metal–organic frameworks for membrane-based separations. Nat Rev Mater 2016;1(12):16078.
[53] Zhao J, Losego MD, Lemaire PC, Williams PS, Gong B, Atanasov SE, et al. Highly adsorptive, MOF-functionalized nonwoven fiber mats for hazardous gas capture enabled by atomic layer deposition. Adv Mater Interfaces 2014;1(4):1400040.
[54] Zhao J, Gong B, Nunn WT, Lemaire PC, Stevens EC, Sidi FI, et al. Conformal and highly adsorptive metal–organic framework thin films via layer-by-layer growth on ALD-coated fiber mats. J Mater Chem A Mater Energy Sustain 2015;3(4):1458–64.
[55] Zhao J, Lee DT, Yaga RW, Hall MG, Barton HF, Woodward IR, et al. Ultra-fast degradation of chemical warfare agents using MOF-nanofiber kebabs. Angew Chem Int Ed Engl 2016;55(42):13224–8.
[56] Zhao J, Nunn WT, Lemaire PC, Lin Y, Dickey MD, Oldham CJ, et al. Facile conversion of hydroxy double salts to metal–organic frameworks using metal oxide particles and atomic layer deposition thin-film templates. J Am Chem Soc 2015;137(43):13756–9.
[57] Zhao J, Kalanyan B, Barton HF, Sperling BA, Parsons GN. *In situ* time-resolved attenuated total reflectance infrared spectroscopy for probing metal–organic framework thin film growth. Chem Mater 2017;29(20):8804–10.
[58] Lee DT, Jamir JD, Peterson GW, Parsons GN. Water-stable chemical-protective textiles via euhedral surface-oriented 2D Cu-TCPP metal–organic frameworks. Small 2019;15(10):e1805133.
[59] Bechelany M, Drobek M, Vallicari C, Abou Chaaya A, Julbe A, Miele P. Highly crystalline MOF-based materials grown on electrospun nanofibers. Nanoscale 2015;7(13):5794–802.
[60] Drobek M, Bechelany M, Vallicari C, Abou Chaaya A, Charmette C, Salvador-Levehang C, et al. An innovative approach for the preparation of confined ZIF-8 membranes by conversion of ZnO ALD layers. J Membr Sci 2015;475:39–46.
[61] Stassen I, Styles M, Grenci G, Gorp HV, Vanderlinden W, Feyter SD, et al. Chemical vapour deposition of zeolitic imidazolate framework thin films. Nat Mater 2016;15(3):304–10.
[62] Salmi LD, Heikkilä MJ, Puukilainen E, Sajavaara T, Grosso D, Ritala M. Studies on atomic layer deposition of MOF-5 thin films. Microporous Mesoporous Mater 2013;182:147–54.
[63] Lausund KB, Nilsen O. All-gas-phase synthesis of UiO-66 through modulated atomic layer deposition. Nat Commun 2016;7(1):13578.
[64] Lausund KB, Petrovic V, Nilsen O. All-gas-phase synthesis of amino-functionalized UiO-66 thin films. Dalton Trans 2017;46(48):16983–92.
[65] Ahvenniemi E, Karppinen M. Atomic/molecular layer deposition: a direct gas-phase route to crystalline metal–organic framework thin films. Chem Commun 2016;52(6):1139–42.
[66] Ahvenniemi E, Karppinen M. *In situ* atomic/molecular layer-by-layer deposition of inorganic–organic coordination network thin films from gaseous precursors. Chem Mater 2016;28(17):6260–5.
[67] Tanskanen A, Karppinen M. Iron-terephthalate coordination network thin films through *in-situ* atomic/molecular layer deposition. Sci Rep 2018;8(1):8976.
[68] Nisula M, Linnera J, Karttunen AJ, Karppinen M. Lithium aryloxide thin films with guest-induced structural transformation by ALD/MLD. Chemistry 2017;23(13):2988–92.
[69] Li K, Olson DH, Seidel J, Emge TJ, Gong H, Zeng H, et al. Zeolitic imidazolate frameworks for kinetic separation of propane and propene. J Am Chem Soc 2009;131(30):10368–9.
[70] Ma X, Kumar P, Mittal N, Khlyustova A, Daoutidis P, Mkhoyan KA, et al. Zeolitic imidazolate framework membranes made by ligand-induced permselectivation. Science 2018;361(6406):1008–11.
[71] Loyer F, Frache G, Choquet P, Boscher ND. Atmospheric pressure plasma-initiated chemical vapor deposition (AP-PiCVD) of poly(alkyl acrylates): an experimental study. Macromolecules 2017;50(11):4351–62.
[72] Loyer F, Bengasi G, Frache G, Choquet P, Boscher ND. Insights in the initiation and termination of poly(alkyl acrylates) synthesized by atmospheric pressure plasma-initiated chemical vapor deposition (AP-PiCVD). Plasma Process Polym 2018;15(5):1800027.
[73] Stair PC, Marshall C, Xiong G, Feng H, Pellin MJ, Elam JW, et al. Novel, uniform nanostructured catalytic membranes. Top Catal 2006;39(3–4):181–6.
[74] Venkatesan BM, Dorvel B, Yemenicioglu S, Watkins N, Petrov I, Bashir R. Highly sensitive, mechanically stable nanopore sensors for DNA analysis. Adv Mater 2009;21(27):2771–6.
[75] Zhang J, Xu W, Liu W. Oxygen-selective immobilized liquid membranes for operation of lithium–air batteries in ambient air. J Power Sources 2010;195(21):7438–44.
[76] Beneq WCS 600 [Internet]. Espoo: Beneq; c2005–19 [cited 2019 May 2]. Available from: https://beneq.com/en/thin-films/products/roll-roll-ald/beneq-wcs-600.
[77] Malinen V, Cook A. Beneq roll-to-roll ALD in practice [Internet]. Espoo: Beneq; 2017 [cited 2019 May 2]. Available from: https://beneq.com/en/thin-films/research-world/science-letters/beneq-roll-roll-ald-in-practice.
[78] Higgs DJ, DuMont JW, Sharma K, George SM. Spatial molecular layer deposition of polyamide thin films on flexible polymer substrates using a rotating cylinder reactor. J Vac Sci Technol, A 2018;36(1):01A117.